Available online at www.sciencedirect.com
SCIENCE DIRECT®
Engineering Fracture Mechanics 71 (2004) 2589–2605
Engineering Fracture Mechanics
www.elsevier.com/locate/engfracmech

Fracture behaviour of 2D-weaved, silica–silica continuous fibre-reinforced, ceramic–matrix composites (CFCCs)

N. Eswara Prasad *, Sweety Kumari, S.V. Kamat, M. Vijayakumar, G. Malakondaiah

Defence Metallurgical Research Laboratory, PO Kanchanbagh, Hyderabad 500058, India

Received 18 February 2003; received in revised form 29 January 2004; accepted 24 February 2004

Abstract

Significantly improved fracture resistance (in terms of fracture toughness and fracture energy) can be imparted to monolithic ceramics by adopting composite design methodology based on fibre reinforcement technology. The present paper describes the fracture behaviour of one such fibre-reinforced material, namely the silica–silica based continuous fibre-reinforced, ceramic–matrix composite (CFCC) in two orthogonal notch orientations of crack divider and crack arrester orientations. Different fracture resistance parameters have been evaluated to provide a quantitative treatment of the observed fracture behaviour. From this study, it has been concluded that the overall fracture resistance of the CFCC is best reflected by total fracture energy release rate (J_c), which parameter encompasses most of the fracture events/processes. The J_c values of the composite are found to be more than an order of magnitude higher than the energy values corresponding to the plane strain fracture toughness (J_{KQ}, derived from K_{Ic}, the plane strain fracture toughness) and >200% higher than elastic–plastic fracture toughness (J_{Ic}). Apart from this, the composite is found to exhibit high degree of anisotropy in the fracture resistance and also, a significant variation in the relative degree of shear component with crack extension.

Keywords: Continuous fibre 2D silica–silica composites; Fracture behaviour and modes of failure; Fracture resistance; Total fracture energy release rate; *R*-curve behaviour

1. Introduction

Ceramic materials have assumed significant technological importance as structural materials because the newer design and development methodologies, adopting fibre reinforcements, have resulted in enhancement of the fracture resistance of monolithic ceramics by several fold [1–6]. Among various ceramic materials, amorphous silica uniquely combines different properties to suit several select technological applications

* Corresponding author. Tel.: +91-40-24340051; fax: +91-40-24340683/4341439.
E-mail addresses: nep@dmrl.ernet.in, neswarap@rediffmail.com (N. Eswara Prasad).

0013-7944/$ - see front matter © 2004 Elsevier Ltd. All rights reserved.
doi:10.1016/j.engfracmech.2004.02.005

[7–10]. These properties include, high melting point combined with high thermal shock resistance and excellent thermal as well as electrical insulating properties [8,10]. However, the mechanical properties of silica material in the monolithic form are far from acceptable levels. Silica, in its bulk form, has low strength (both tensile and flexural) and extremely low fracture toughness as compared to several structural ceramic materials [8]; thus, needing significant improvements so that it can be accepted for any structural application. One of the means of achieving improved mechanical properties is by using either two- or three-dimensional (designated commonly as 2D- and 3D-, respectively) networks of continuous fibres as reinforcements to the ceramic–matrix material leading to newer structural materials, known as "continuous fibre-reinforced, ceramic–matrix composites (CFCCs)". Numerous studies have been conducted in the last two decades on the fibre/whisker toughening of this class of ceramics. These studies have been comprehensively reviewed by Evans [2] as well as by Becher [4] and later, by Faber [6]. However, to the best of our knowledge, there are no fracture toughness/energy studies reported so far for the silica–silica CFCCs.

During the fracture process of a CFCC, various events/developments take place in the three regions of the fracture, namely the wake of the crack, at the crack tip and finally in the region of process zone ahead of the crack tip. These influence the net enhancements in the fracture resistance of a CFCC. They include some or most of the following [2,3,5]:

1. Local increase in the stress level with the application of external loading,
2. relative displacement of matrix/interface elements,
3. matrix microcracking, leading to matrix failure (with or without significant crack path meandering, i.e., crack deflection and/or branching),
4. debonding of matrix/fibre interface (with or without significant frictional forces),
5. fibre pull-out and fibre breakage in the crack tip process zone,
6. frictional sliding of the fibres along the matrix/fibre interfaces,
7. loss of residual strain energy.

These processes/stages, schematically shown in Fig. 1, result in significant energy dissipation through frictional events in the wake and process zones, acoustic emission and fibre debonding, pull-out and breakage. Contributions from these stages of crack tip and fibre reinforcements interactions, with or

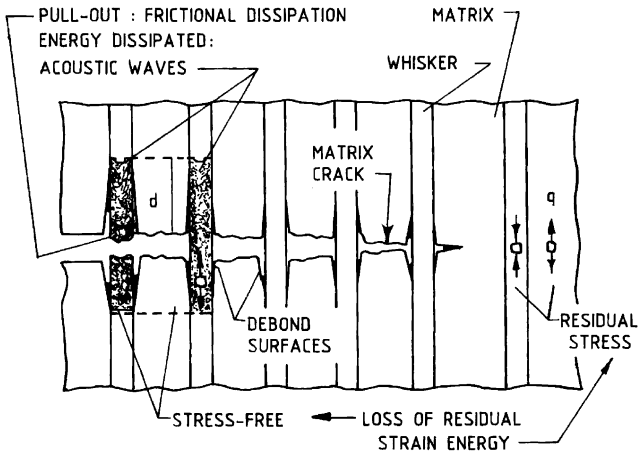

Fig. 1. Schematic showing various events and processes of crack bridging mechanism in fibre-reinforced composites (from Ref. [2]). Note that the crack extension process essentially involves matrix microcracking, fibre/matrix debonding, fibre fracture and fibre pull-out.

without the contributions from matrix fracture events, have led to unified models for the fracture resistance in materials that exhibit crack bridging [2–6]. The toughening in these cases of crack bridging is essentially due to ductile or brittle reinforcements. In the case of present CFCCs, it is the later that makes contributions to the toughening.

In the present paper, the fracture behaviour of a two-dimensional (2D) silica fibre-reinforced, silica–matrix composite is presented and discussed. Various parameters of fracture resistance have been used to quantify the fracture resistance of the material. These include, the plane strain fracture toughness (K_{Ic}), elastic–plastic fracture toughness (J_{Ic}) and total fracture energy release rate (J_c). Also reported and discussed are the effects of notch orientation and notch depth on the fracture resistance in these composites.

2. Experimental details

The two-dimensionally weaved silica fibre preforms are vacuum impregnated using colloidal silica solution precursor to provide the matrix for the silica–silica continuous fibre-reinforced, ceramic–matrix composites (referred to as "silica–silica CFCC" or simply "CFCC"). The interconnected network of capillaries in the preforms facilitates solution impregnation, thus providing uniform matrix for the CFCC. After infiltration, the CFCC is dried and during this drying process, water content of the matrix gel solution is gradually removed. These dried CFCCs are then sintered to impart interparticle bonding and in turn, this facilitates load transfer from the matrix to the fibre and vice-versa.

There are no standard test procedures for the evaluation of fracture toughness/energy of ceramic materials, especially for the advanced ceramic composites such as CFCCs. However, several studies have been reported in the recent past which describe in detail the procedures adopted for and the fracture behaviour observed of the monolithic ceramics and ceramic–matrix composites, including CFCCs (see Refs. [11–18] for details and a summary of these details in Ref. [19]). Since ceramic materials exhibit brittle fracture, the ASTM Standard E-399, describing the standard practice for the evaluation of plane strain fracture toughness of metallic materials [20], can conveniently be adopted to determine the fracture toughness of these materials. However, since the CFCCs also exhibit limited extent of non-linear fracture, the J-integral technique once again developed for metallic materials (fundamentals and standard practices described in Refs. [21–23] and [24], respectively) also applies equally.

Single edge notch beam (SENB) specimens of 8 mm thickness, 10 mm width and a span length of 40 mm were used. The fracture toughness/energy was evaluated in two notch orientations, namely (i) crack divider orientation, in which the notch is along the orientation of the plies in the thickness direction and (ii) crack arrester orientation, in which the notch is perpendicular to the orientation of the plies in the thickness direction (the third orientation of crack delamination could not be studied because of specimen size limitations). In both cases, notch is perpendicular to the longitudinal plies.

Notches of varied length were introduced using 0.3 mm thick diamond wafer blades, mounted on a standard Isomet cutting machine. A specially designed jig was used to obtain straight notches by moving the job across the cutting plane. The notches thus introduced were found to have a finite root radius, ρ, typically of the order of 160 μm. The ρ values were determined by Delta TM 35 x–y profile projector. The notch root radii, either in the crack divider or crack arrester orientation, were found to be similar. The crack lengths were maintained in the range of 0.35 to 0.7 times the specimen width. Among these, specimens with crack lengths in the range specified by the ASTM standard E-399 [20] (0.45–0.55 times the specimen width) were only considered for the determination of K_{Ic} values. The other specimens with larger crack lengths were employed essentially to determine the work of fracture [25], which results will be reported separately. The fracture energy determined from the load–displacement data were used to determine the elastic–plastic fracture toughness, J_{Ic} and the total fracture energy release rate, J_c. The later two fracture resistance parameters are based on J-integral [21].

All the fracture toughness tests were conducted on a computer controlled, servohydraulic Instron 8801 test system using a self-articulating 3-point bend fixtures of MTS 880 test system. The tests were conducted at ambient temperature (~23 °C) and in laboratory air atmosphere. The notched specimens were loaded in ramp control at a constant ramp rate of 0.5 mm/min. The load–displacement curves thus obtained were analysed to obtain various measures of fracture resistance, and the results are presented and discussed in the following sections.

3. Results and discussion

3.1. Load–displacement data and crack path observations

The load–displacement data obtained for crack divider and crack arrester orientations are shown in Figs. 2 and 3, respectively. Crack lengths are given as normalised values (crack length 'a', normalised with the specimen width, 'W'). Though six tests with different a/W values were conducted in the crack arrester direction, for the sake of clarity, only three load–displacement plots are included in Fig. 3. On the other hand, all the four load–displacement plots obtained are included in Fig. 2 for the crack divider direction.

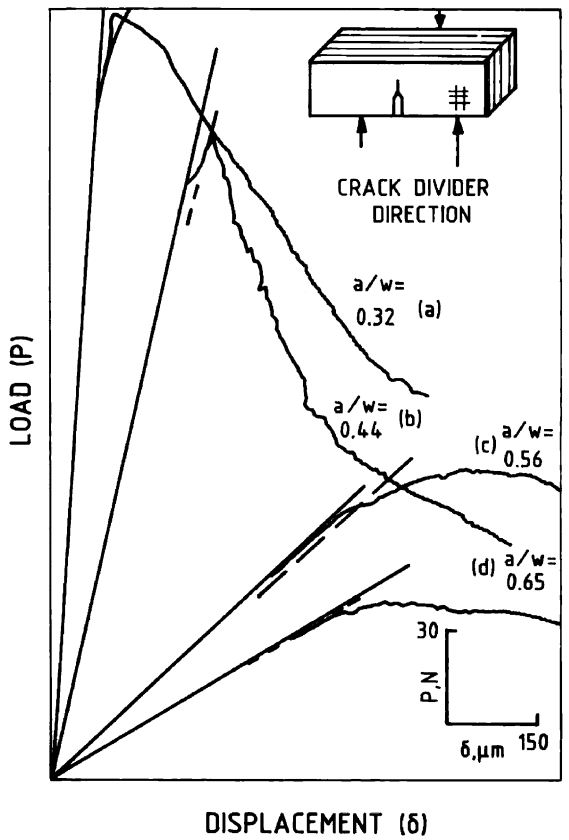

Fig. 2. Load–displacement data obtained during the evaluation of fracture resistance using specimens with varied crack length (given in terms of the normalised crack length with specimen width) in case of the material in the ''crack divider'' orientation.

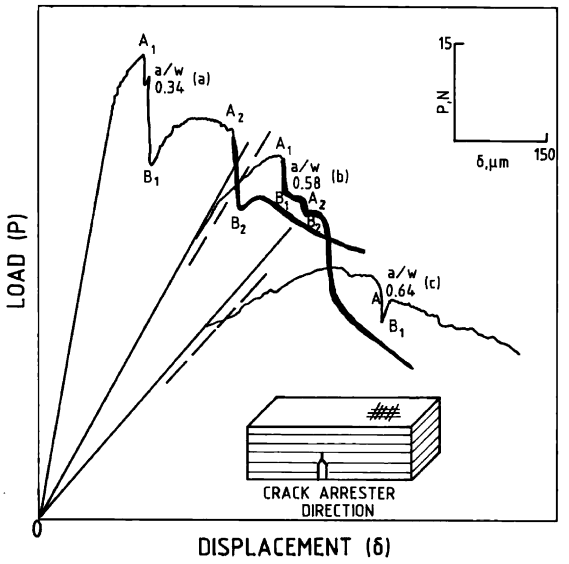

Fig. 3. Load–displacement data obtained during the evaluation of fracture resistance using specimens with varied crack length (given in terms of the normalised crack length with specimen width) in case of the material in the "crack arrester" orientation.

It can be seen from these curves that increase in crack length decreases maximum load attained prior to the commencement of crack extension. The load initially increases linearly with the displacement in all the cases. This corresponds to the stage in which the specimen largely experiences elastic stresses. Followed by this stage, the crack extension takes place. This is reflected in nonlinear increase in the load with displacement followed by noticeable drop in the load with further increase in the displacement. The load–displacement curves show distinctly different characteristics at this stage of crack extension in the two notch orientations.

The material in the crack divider orientation shows a steep, but continuous fall in the load with increase in the displacement (Fig. 2). Such a behaviour is seen in specimens with lower crack lengths ((a) and (b) in Fig. 2 with $a/W = 0.32$ and 0.44, respectively). This clearly indicates gradual extension of the crack front. However, higher crack length specimens in this notch orientation ((c) and (d) in Fig. 2 with $a/W = 0.56$ and 0.65, respectively) do not show such steep load drop. Instead, these specimens show near-saturation in the variation of load with displacement, up to a displacement of $\sim$800 μm. In this case, the fibre bundles undergo significant bending without breakage and crack extension essentially occurs along fibre/matrix interface. On the other hand, the specimens in the crack arrester orientation show distinct and sudden load drops with crack extension (shown as A_1B_1, A_2B_2 etc., in the curves (a), (b) and (c) of Fig. 3). Again, at large crack lengths ($a/W = 0.64$, case (c) in Fig. 3) the specimen shows gradual load drop with displacement. Such a behaviour is attributable to the change in the nature of crack extension. As shown schematically in Fig. 4a, the specimens in the crack arrester orientation show complete mode I (tensile) fracture with predominant fibre bundle breakage leading to relatively insignificant crack extension along the fibre/matrix interface when the crack lengths are smaller ($a/W < 0.45$). As crack length increases, the extent of crack extension along the fibre/matrix interface also increases, leading to significant extent of '*H*' and '*T*' cracking (Fig. 4b). This results in mode I crack extension in the initial stages and a mixed mode fracture in the later stages, comprising mode I and mode II (in-plane shear or sliding) components. This occurs in case of specimens with a/W values in the range 0.55–0.6. At still higher crack lengths (cases (c) and (d) in Fig. 2 and (c) in Figs. 3 and 4), the crack extension occurs essentially in mode II with interply shearing being the

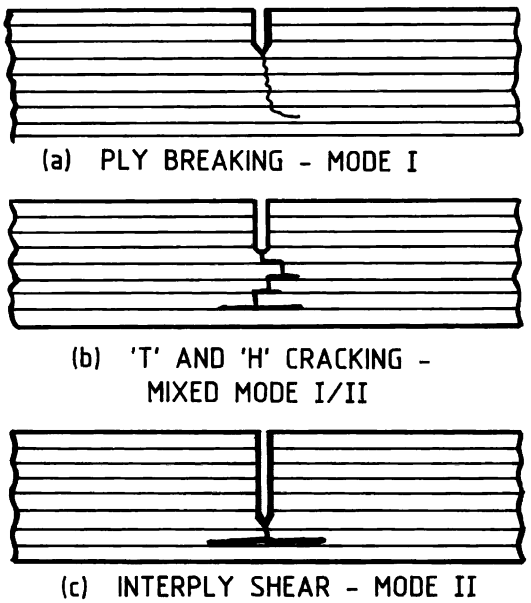

Fig. 4. Schematic figure showing the nature of crack extension in the crack arrester orientation when the specimen crack length is varied significantly. (a) Short crack lengths ($a/W < 0.4$), (b) intermediate crack lengths ($0.4 < a/W < 0.55$) and (c) longer crack lengths ($a/W > 0.6$). Note the increasing extent of mode II fracture component with increasing crack length values.

principal fracture event. The associated fibre bundle fracture is negligible (notice the very small sudden load drop(s) shown as A_1B_1 in Fig. 3c).

3.2. Plane strain fracture toughness (K_{Ic})

The plane strain fracture toughness (K_{Ic}) of the 2D silica–silica CFCC material was evaluated in the crack divider and crack arrester orientations according to the ASTM standard E-399 [20]. Specimens of varied crack length have been used for the determination of fracture toughness. Figs. 2 and 3 show the basic data of the load variation with displacement for the specimens in the two notch orientations. Table 1 provides the details of the specimens and the data derived from these fracture toughness tests. Though the specimens with varied a/W were tested, data corresponding to specimens with a/W values in the range of 0.45–0.55, as specified by ASTM standard E-399 [19], were only used to arrive at K_{Ic}. The values of K_{max} and K_Q derived for each test are also listed in Table 1. These data in Table 1 show that the material exhibits valid K_{max}/K_Q values (<1.1) only when the crack lengths are smaller ($a/W < 0.44$). At higher crack lengths, the material exhibits limited extent of stable crack extension, which yielded K_{max}/K_Q values that are in excess of 1.1. In view of these observations, the K_Q values derived from specimens with a/W of 0.44 and 0.56 in the crack divider orientation and 0.52 in the crack arrester orientation (note only a small variation in the K_Q values between different test specimens, see data in Table 1) are considered to yield valid K_{Ic}.

Under such conditions, the CFCC material exhibits a significantly higher fracture toughness value in the crack divider orientation as compared to the crack arrester orientation. An average value of 2.03 MPa $\sqrt{m}$ (corresponding to the crack lengths of a/W of 0.44 and 0.56) obtained for the crack divider orientation is more than 100% higher than the value obtained in the crack arrester orientation ($K_{Ic} = 0.98$ MPa $\sqrt{m}$). Secondly, the value of conditional fracture toughness (K_Q) decreases significantly with increase in the crack length, especially in the crack divider orientation. This is due to the change in fracture mode. At higher

Table 1
Plane strain fracture toughness (K_{Ic}, MPa $\sqrt{m}$) data of the 2D silica–silica CFCC material

Specimen no.	W	B	a and a/W	$f(a/W)$	P_Q and P_{max}	K_Q and K_{max}
(a) Crack divider orientation						
1	9.76	7.23	3.12 and 0.32	1.6	234 and 246	2.15 and 2.26
2	9.93	7.54	4.39 and 0.44	2.22	205 and 206	2.43[a] and 2.43
3	9.94	7.17	5.60 and 0.56	3.25	89 and 101	1.63[a] and 1.84
4	9.76	7.26	6.35 and 0.65	4.63	52 and 58	1.36 and 1.52
(b) Crack arrester orientation						
1	7.76	7.60	2.52 and 0.325	1.62	70 and 74	0.86 and 0.90
2	7.74	7.53	2.7 and 0.35	1.73	58 and 66.5	0.78 and 0.89
3	7.59	8.95	3.06 and 0.403	2.15	58 and 60	0.84 and 0.87
4	7.68	9.13	4.0 and 0.52	2.84	53 and 60	0.98[a] and 1.10
5	7.61	9.76	4.84 and 0.58	3.5	33 and 40	0.72 and 0.86
6	7.67	9.89	4.9 and 0.64	4.43	37 and 49	0.99 and 1.3

W—specimen width, in mm; B—specimen thickness, in mm; L—specimen span length (fixed value of 40 mm); P_Q—conditional load for the onset of fracture, in N; P_{max}—maximum load in the load–displacement curve, in N; K_Q—conditional fracture toughness, in MPa $\sqrt{m}$; K_{max}—maximum stress intensity factor, in MPa $\sqrt{m}$.
[a] Valid K_{Ic}.

crack lengths, as discussed in the previous section, the fracture mode gradually changes to predominant shear, involving mode II (in-plane shear or sliding) fracture components. This is true for both test orientations.

3.3. Elastic–plastic fracture toughness (J_{Ic})

The procedure suggested by Landes and Begley [23] and the ASTM standard E-813 [24] provide details of the latest standard practice for the determination of elastic–plastic fracture toughness, J_{Ic}. Alternatively, another widely accepted methodology, again suggested by Landes and Begley [22], can also be employed for J_{Ic} determination. Both these methodologies are based on Rice proposed J-integral [21]. The later procedure principally involves the determination of fracture energy (J_Q) from the energy absorbed in the fracture process (E_{ini}, area under the load–displacement, usually the displacement considered here corresponds to the load line) by specimens with different crack lengths, up to either a constant displacement or a constant load. In the present case, the load–displacement data given in Figs. 2 and 3 are used to calculate the energy for the crack initiation (E_{ini}), which event is assumed to occur at the displacements corresponding to the peak load. E_{ini} values thus determined are used to calculate the fracture energy, J_Q as [21,22]:

$$J_Q = \Delta E_{ini}/B(\Delta a), \tag{1}$$

where (ΔE_{ini}) is the difference in the fracture energies (corresponding to peak loads in the load displacement curves) of two specimens with different initial crack lengths (their difference is Δa). The values of J_Q, determined from the load–displacement curves in crack divider and crack arrester orientations, are shown as a function of crack length in Fig. 5. As to be expected, the material shows constant values of J_Q in the crack divider (1.36 kJ/m^2) and crack arrester (0.66 kJ/m^2) orientations. The scatter in J_Q values is higher for crack arrester orientation as compared to the crack divider orientation. However, all these values were found to satisfy the validity conditions and hence, can be termed as elastic–plastic fracture toughness, J_{Ic} of the CFCC.

As stated above, the J_{Ic} corresponds to the peak load (assumed to correspond to the crack initiation) and hence would encompass only those fracture events that occur in the CFCC material before or up to the

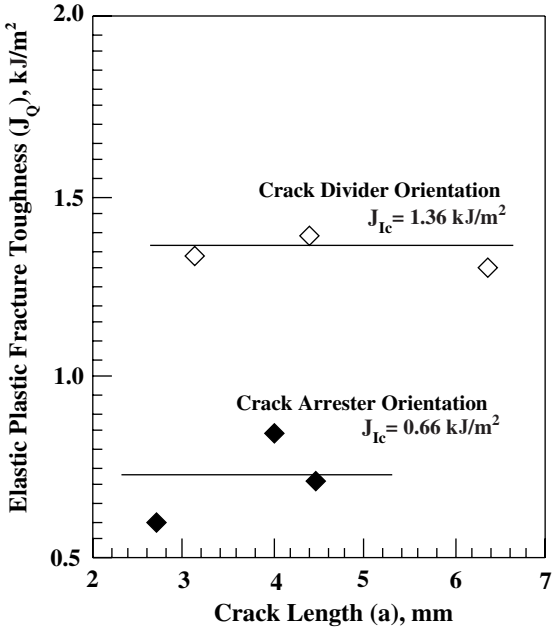

Fig. 5. Variation of elastic–plastic fracture toughness (J_Q) with crack length for the CFCC in crack divider and crack arrester orientations.

event that the material undergoes first fibre bundle fracture. As discussed earlier, these events include matrix microcracking and fibre/matrix debonding; but, do not include the fibre bundle failure and fibre pull-out. However, it is well accepted now that the last two events too contribute significantly to the overall fracture resistance of CFCC materials and the energy absorbed during these two processes is also considerable. Hence, an alternative method of total (elastic–plastic) fracture energy release rate is adopted to evaluate the fracture resistance that accounts for all the fracture events of the present material (described in details in the next section). Hence, the J_{Ic} values evaluated and reported in the present section are valid materials' fracture resistance properties; however, they are conservative in nature.

3.4. Total fracture energy release rate (J_c)

Li and coworkers [26–29] have successfully extended the J-integral concept to brittle materials, first for concrete materials and later for inhomogeneous and discontinuous materials, a preliminary review of which was provided by Mai [30]. Later, these methodologies were successfully employed for CFCCs by Li and coworkers themselves [29] and Nair and Wang [31]. Homogeneous materials exhibit a parabolic decrease in the stress with radial distance (r) from the crack tip (Fig. 6a). Such a gradual decrease in the stress denotes stable crack extension, which is one of the basic requirements for applying J-integral. The discontinuous, heterogeneous CFCCs also exhibit such crack tip stress singularity. But these materials, in addition, exhibit events of unstable crack extension. This is despite the fact that the material, in general, exhibits parabolic decrease in the stress with radial distance, r (Fig. 6b). Each of the load excursions and sudden load drops in Fig. 6b represent the local crack tip fracture event. A sudden load drop in the crack tip stress level is due to the failure of a fibre bundle and the subsequent load excursion is due to gradual build up of the local stress. In such cases, the overall or global fracture energy (J_α or the total fracture energy release rate, J_c) represents the fracture resistance of the material.

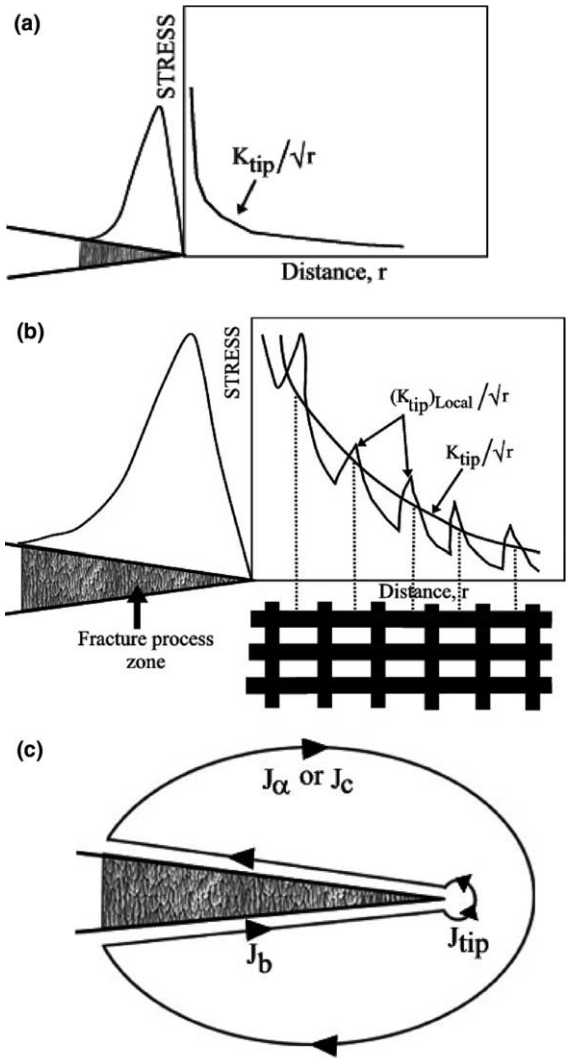

Fig. 6. Schematic diagram showing the crack tip stress singularity for (a) homogeneous material, (b) heterogeneous material, such as CFCCs. (c) J-contour for the heterogeneous material. Note the large wake zone of the heterogeneous material (in b) as compared to the homogeneous material (in a).

The total fracture energy release rate, J_α or J_c, encompasses different stages of fracture events (listed in Section 1) in the "fracture zone" (see Figs. 1 and 6c). In case of homogeneous materials, fracture processes ahead of or at the crack tip predominantly contribute to the overall fracture resistance. Hence, the energy release rate at the crack tip (termed as 'J_{tip}') predominates the values of J_α. On the other hand, the discontinuous materials such as CFCCs, the wake zone effects predominate in comparison with the J_{tip}. Hence, in these cases the overall energy release rate J_α essentially includes fracture energy corresponding to wake zone effects and the contributions from the crack tip processes or crack tip fracture zone (J_{tip}) are only marginal. Further, the total fracture energy release rate (J_c or J_α, or some times referred to as G_c) is the most commonly used parameter when a fracture process involves two or more different components of fracture.

This is the case in the present CFCC materials. As stated earlier, the increasing contributions from mode II or in-plane shear fracture during mode I fracture toughness evaluation using specimens of varied crack length, require the adoption of such an energy concept. Li and coworkers [29] have clearly shown that the total fracture energy release rate (they referred to this parameter as the global or over-all fracture energy release rate, J_α and we designate this term as J_c, the (critical) total fracture energy release rate; see Fig. 6c) corresponding to the far field loading for discontinuous CFCCs and is given as

$$J_c = J_b + J_{tip}, \tag{2}$$

where J_b is the energy consumed by the development of fracture process zone and J_{tip} can be obtained from the stress intensity factor at the crack tip, K_{tip} using the equation:

$$J_{tip} = K_{tip}^2(1 - v^2)/E. \tag{3}$$

The overall fracture energy release rate (J_c) could be obtained from [31,32] (using an equation similar to (1)):

$$J_c = \{-(\Delta E_{fr}/\Delta a)\}/B. \tag{4}$$

$\Delta E_{fr}/\Delta a$ is the slope of the linear regression curve fit between the total energy for fracture (E_{fr}) and the crack length (a). The Δa here is actually the difference in the crack lengths (such as $a_2 - a_1$ or $a_3 - a_1$; where a_1, a_2 and a_3 correspond to the initial crack lengths of different specimens) but not crack extension. Once the two terms of J_c and J_{tip} are calculated individually, the third term J_b can be computed from Eq. (2).

The procedure involved for the evaluation of J_c is illustrated schematically in Fig. 7. Specimens of varied crack length (three crack lengths, a_1, a_2 and a_3, in which $a_1 < a_2 < a_3$ as in the present case of crack arrester orientation) are pulled in tension in ramp control. These values of (E_{fr}) vary with the chosen value of displacement (δ, in this case δ_1, δ_2, and δ_3 (and $\delta_1 < \delta_2 < \delta_3$) as shown in Fig. 7). Ideally, the displacement value is chosen in such a way that it encompasses all the events that significantly influence the fracture process and hence, reflected in the determined total fracture energy release rate. In the present study, three grossly different displacement values (δ_1, δ_2, and δ_3) are chosen for the evaluation of J_c. The first chosen value of the displacement (δ_1) essentially encompasses the elastic region and in this case even the peak load

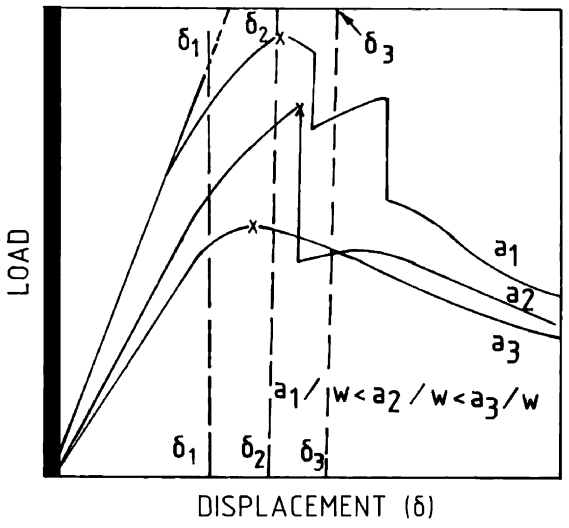

Fig. 7. Representative load–displacement curves showing the procedure adopted for the evaluation of total fracture energy release rate (J_c).

Table 2
Total fracture energy release rate (J_c) of the CFCC material in crack divider and crack arrester orientations

Orientation	Nature shown in	Displacement (δ) (μm)	Slope of the $E_{fr} - a$ regression line (J/m)	J_c (kJ/m^2)	Operative crack bridging mechanisms
Crack divider	(A) in Fig. 8a	$\delta_1 = 130$	4.9	0.67	Matrix cracking
	(B) in Fig. 8a	$\delta_2 = 250$	15.8	2.16	Matrix cracking, fibre/matrix debonding
	(C) in Fig. 8a	$\delta_3 = 720$	26.0	3.56	Matrix cracking, fibre/matrix debonding, fibre breakage and pull-out
Crack arrester	(A) in Fig. 8b	$\delta_1 = 150$	3.0	0.35	Matrix cracking
	(B) in Fig. 8b	$\delta_2 = 400$	5.8	0.68	Matrix cracking, fibre/matrix debonding
	(C) in Fig. 8b	$\delta_3 = 660$	6.8	0.79	Matrix cracking, fibre/matrix debonding, fibre breakage and pull-out

obtained for the specimen with smallest crack length, a_1, is not exceeded. Such low displacement values presumably include the fracture event of matrix microcracking and hence, would indicate the matrix fracture resistance. As would be seen in the following paragraphs this fracture energy $[(J_c)_{\delta 1} = (J_c)_{matrix}]$ is more than 50% lower than the overall fracture energy ($(J_c)_{\delta 3}$) of the composite. The disparity in the J_c values at δ_1 and δ_3 displacements is significantly higher in the crack divider direction as compared to the crack arrester direction (see data in Table 2). The second chosen displacement, δ_2, corresponds to the peak load and hence, encompasses the matrix cracking and the fibre/matrix debonding. However, the most appropriate case is the third chosen displacement, δ_3, which encompasses the first major load drop indicating fibre bundle breakage. Such large displacement effectively would include all the fracture events of significance and hence, provides the highest values of J_c.

The above procedure has been followed to evaluate the total energy release rate (J_c) of the present CFCC material. The variation of fracture energy (E_{fr}) determined for the CFCC material is shown as a function of crack length in Fig. 8a and b, respectively for crack divider and crack arrester orientations. The E_{fr} values derived here are similar to the E_{ini} values, derived for J_{Ic} evaluation (see previous section). In the former case, the E_{fr} is energy till a certain displacement value; while, the latter E_{ini} is the energy till the specimen attains peak load. In both the notch orientations, the higher values of displacements considered yielded higher fracture resistance, J_c. The slope values ($E_{fr}/\Delta a$) and the corresponding J_c values vary significantly with the value chosen for the displacement δ (see data in Table 2). The fracture energy progressively

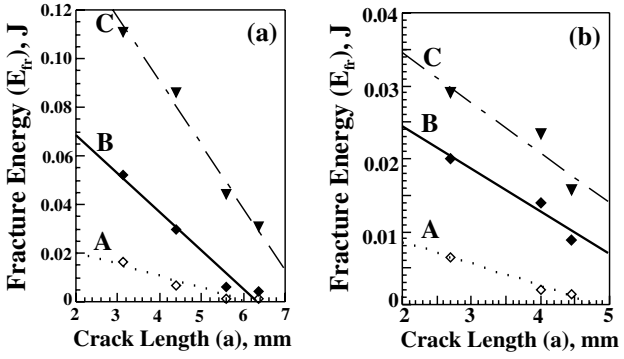

Fig. 8. Variation of fracture energy (E_{fr}) with the crack length for three different crack displacement values (δ_1, δ_2 and δ_3 for cases of A, B and C, respectively; for details see Table 2) for the CFCC material in (a) crack divider and (b) crack arrester orientations. Note the increase in the slope of the linear curve fit with increasing δ, indicating the increase in the value of total fracture energy release rate with crack extension.

increases with increase in the displacement as higher displacements include more fracture processes and events that enhance the fracture resistance of these materials. Microstructural observations of the fractured specimens have shown that the cracks in all the three cases of varied crack length extend in the shear mode; not, in the intended tensile mode, once a displacement of value of about 600–800 μm (depending on the initial crack length, termed here as the maximum stable displacement, δ_{max}) is reached. Hence, no displacements are considered for the J_c evaluation in the present study, which are in excess of this δ_{max} value. Further, in the displacement region where shear fracture is dominant, any further crack extension (increase in the displacement, δ) does not significantly increase the total fracture energy release rate (J_c). It is also observed that soon after the event of first fibre bundle fracture, the crack front becomes unstable; but, the specimen regains stability (shown as the increase in the load with crack extension) after crack extension of a few tens of microns. We have chosen the displacement value at which such an unstable/stable crack extension occurs as the critical displacement value δ_c. This δ_c is taken as the one corresponding to the average δ at peak load of the three or four specimens that are tested with different initial crack lengths. A δ_c value of 260 μm for crack divider orientation and 400 μm for crack arrester orientation are found to be appropriate for the present case. The derived values of total fracture energy release rate at varied displacements (given as displacements normalised by the δ_c) are shown in Fig. 9 for the CFCC material in the crack arrester orientation. The data in Fig. 9 clearly show that the CFCC material exhibits maximum fracture energy, asymptotic values of J_c of 3.6 and 0.84 kJ/m^2 for crack divider and crack arrester orientations, respectively.

It should be noted here that the standard J_{Ic} evaluation procedures for the metallic materials [21–24] do not recommend the practice of using the calculated fracture energies for such large displacements as δ_3 for two reasons. Firstly, the sudden load drop corresponding to the breakage of a minimum of one fibre bundle is actually an event of unstable crack extension. (Though, this could be contested on the basis of the

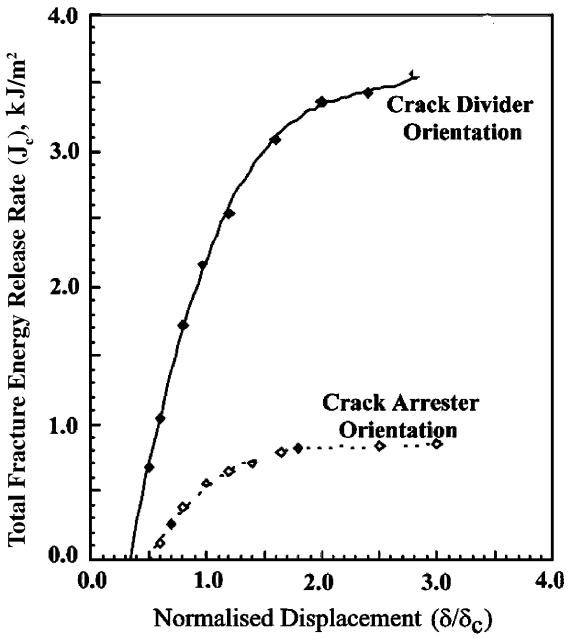

Fig. 9. Variation of total fracture energy release rate with normalised displacement in case of the CFCC material in the two notch orientations. Note the asymptotic values of J_c of 3.6 and 0.84 kJ/m^2 respectively, represent the maximum fracture energies for the material in two notch orientations of crack divider and crack arrester orientations.

observation that the major load drops observed in the present study are followed by an increase in the load with the subsequent crack extension, which indicates that the subsequent crack growth occurs in a stable manner.) Secondly, the mode of fracture is not the same for the various combinations of crack length (a) and displacement (δ). For lower crack lengths and small displacements (as in the case of specimens with a_1 and a_2 crack lengths and δ_1 displacement), the mode of failure is purely mode I or tensile. On the other hand, for large crack length (a_3) specimens and large displacement (δ_2 and δ_3) values, the mode of fracture involves significant mode II or in-plane shear component of fracture.

3.5. Comparison of various fracture toughness parameters

The present CFCC material is isotropic in the in-plane directions. Hence, we assume that the following equation to derive the fracture energy (J_{KQ}) from the K_{Ic} values [33] is valid:

$$(J_{KQ}) = K_{Ic}^2(1 - v^2)/E, \tag{5}$$

where v is the Poisson's ratio, whose value was assumed to be 0.3 for both the orientations. The values of elastic modulus (E) were experimentally measured as 18.8 GPa in the two in-plane directions [34]. The J_{KQ} values derived from K_{Ic} are up to an order of magnitude lower (333 J/m^2 in the crack divider orientation and 47 J/m^2 in the crack arrester orientation) than the J_{Ic} and J_c values (the maximum value of J_c in the crack divider orientation is 3.6 kJ/m^2). This is because the K_{Ic} or the J_{KQ} includes the fracture events at the most up to first fibre bundle failure (mostly confined to the events of matrix microcracking) and does not include any further events of crack–reinforcement interactions.

Finally, all the three fracture resistance parameters, namely the J_{KQ} (fracture energy value corresponding to the K_{Ic}), J_{Ic} and the J_c values, determined in the present study for the two notch orientations are compared in Table 3. This data comparison clearly reveals that the K_{Ic} values grossly underestimate the fracture resistance of the material as compared to J_{Ic} or J_c values. The J_{Ic} values, themselves are 2 to 3 times lower as compared to the J_c values, a finding that demonstrates the effectiveness of the fibre bundle failure and the related increase in the fracture resistance by crack bridging. This is reflected in the values of J_b, the energy consumed in the development of the wake zone (3.27 kJ/m^2 in crack divider orientation and 0.79 kJ/m^2 in the crack arrester orientation), whose values compare very well with the J_c values and are considerably higher than the J_{Ic} values. This indicates that the present CFCC material exhibit large degree of nonlinear fracture region with pronounced R-curve effects, with large fracture energies that are involved in the creation of a highly effective fracture zone at the wake of the crack tip, a behaviour that nearly matches with the recent results reported in the case of 2D SiC/SiC CFCCs [31]. In view of the above, it is appropriate to consider the J_c values of the material and refer to these values as the most effective design parameter.

3.6. Anisotropy in fracture resistance

Major differences in the fracture behaviour of the present CFCC material in the two orthogonal notch orientations of crack divider and crack arrester orientations are described in the preceding paragraphs.

Table 3
Fracture toughness parameters of the CFCC material, values evaluated in the present study

S. no.	Description	Crack divider orientation	Crack arrester orientation
1.	Plane strain fracture toughness (K_{Ic}), MPa $\sqrt{m}$	2.03	0.98
	And equivalent J_{KQ} or J_{tip}, kJ/m^2	0.333	0.047
2.	Mode I, elastic–plastic fracture toughness, (J_{Ic} or J_Q), kJ/m^2	1.36	0.66
3.	Total fracture energy release rate (J_c), kJ/m^2	3.6	0.84

From these, it is evident that the fracture behaviour of the CFCC in terms of nature of load–displacement curves, values of various fracture toughness parameters (see Table 3) and finally, the nature of crack extension, are grossly different for the two notch orientations. Such differences are more clearly reflected in the variation of total fracture energy release rate (J_c) with the extent of crack extension (δ/δ_c), as depicted in Fig. 9. These could be termed as *R*-curves. These fracture resistance curves show that the material exhibits pronounced *R*-curve effects (the net increase in fracture resistance with crack extension), indicating significantly higher fracture resistance (both in terms of initiation ($\delta/\delta_c < 1$) and propagation ($\delta/\delta_c > 1$) fracture resistance values) in crack divider orientation as compared to crack arrester orientation. At any value of δ/δ_c, the J_c in the crack divider orientation is more than 4–5 times higher. Further, the *R*-curve in the crack divider orientation is highly rising in nature, while the same in the crack arrester orientation is relatively flat. These observations clearly point to the fact that crack bridging is all the more effective in the crack divider orientation, in which orientation the fracture resistance of the CFCC is significantly higher.

4. Comparison of fracture resistance

It is interesting to note that the silica materials, first ever explored for any advanced structural application, are in the form of ultra light weight (96–352 kg/m^3; highly porous) fibrous ceramic thermal insulating structures. The first comprehensive studies on the mechanical properties of these structures were carried out by Newman in the early 1980s [35]. Green et al. [36–38], Komine and Kobayashi [39,40] and more recently by Ortiz-Longo and White [9] have comprehensively evaluated the fracture resistance of these materials. A comparison of the fracture toughness properties of these porous materials with those reported in the present study show that the present CFCC material is much superior (though the present CFCC material is also porous, it is much denser (2250 kg/m^3) in comparison). The conservative estimate of the plane strain fracture toughness, K_{Ic} of the present CFCC material (2.03 MPa $\sqrt{m}$ in the crack divider orientation) itself is nearly two orders of magnitude higher than the fracture resistance values reported for these (highly porous) fibrous structural materials. The fracture toughness values (K_{Ic} or K_R) of these materials are in the range of 12–160 kPa $\sqrt{m}$, depending on the process condition, fibre characteristics, notch orientation and finally, the test temperature [9,36–40]. In another study, Hashida et al. [29] have reported the fracture energy values of several glass-matrix-based CFCCs. These fracture energy values (3.5–242 J/m^2; see Table 2 in Ref. [29]) vary significantly depending on the combination of the matrix and the reinforcement characteristics. The reported fracture energy values include the crack propagation events and hence, represent the highest possible fracture energy values. The J_c values of the present CFCC material are more than an order of magnitude higher as compared to this class of CFCCs. However, it should be noted here that the K_{Ic} values of these glass-matrix CFCCs compare well with the K_{Ic} values of the present CFCC material (see data in Tables 2 and 3 of Ref. [29]). Hence, this data comparison clearly illustrates again that the crack tip fracture processes (which essentially influence the K_{Ic} values) contribute to a small extent to the overall fracture resistance and when the further fracture events of crack extension processes such as fibre bundle failure are included, the total fracture energy release rate values become significantly higher.

Finally, the K_{Ic} of the present CFCC material (2.03 MPa $\sqrt{m}$ in the crack divider orientation and 0.98 MPa $\sqrt{m}$ in the crack arrester orientation) compare favourably only with monolithic fused silica (0.74 MPa $\sqrt{m}$) [8]. This again signifies the fact that until all the fracture events other than the matrix microcracking are considered, the fracture resistance of the present CFCC material in terms of K_{Ic} appears limited. The K_{Ic} values of these silica materials, either in the form of fused silica or CFCC are 100–200% lower as compared to the other structural ceramics ($K_{Ic} \sim$ 3–5 MPa $\sqrt{m}$) and are nearly 10 times lower as compared to the high strength, high performance CFCCs based on the SiC/SiC materials [31,41–44] ($K_{Ic} \sim$ 20–30 MPa $\sqrt{m}$, the best values reported till date for specimens with long cracks). However, these

SiC/SiC CFCCs themselves have 2–5 times lower values of fracture energy as compared to the traditional structural superalloys ($J_{Ic} \sim 80$–160 kJ/m^2) [44].

5. Conclusions

The 2D silica–silica CFCC material has been comprehensively evaluated for its fracture resistance. These properties pertain to the values at ambient test temperatures. The significant findings are:

1. The silica–silica CFCC material exhibits a grossly different nature of variation in the load with displacement in crack divider and crack arrester orientations. The later direction clearly exhibits a distinct feature of fibre bundle failure and crack arrest in the form of sudden load drop (corresponding to the fibre bundle failure), its arrest and subsequent increase in the load. On the other hand, the load drop with the crack extension (increasing displacement after the attainment of maximum load) is steep, but, gradual for crack divider orientation.
2. The K_{Ic} values determined for the material are conservative in nature. The values determined are 2.03 MPa $\sqrt{}$m in the crack divider orientation and 0.98 MPa $\sqrt{}$m in the crack arrester orientation. The corresponding fracture energy (J_{KQ}) value are also significantly lower—more than an order of magnitude, as compared to the other two fracture energy values (J_{Ic} and J_c). The values of elastic–plastic fracture toughness (J_{Ic}) are found to be intermediate to the J_{KQ} and J_c values in the two notch orientations.
3. The (critical) total fracture energy release rate values of the present CFCC material approach an asymptotic value of 3.6 kJ/m^2 for crack divider orientation and 0.84 kJ/m^2 crack arrester orientation. These values are best representative of the material's fracture resistance and found to include all the events of the fracture process, principally, the matrix microcracking, debonding of fibres from the matrix, fibre bundle failure and the subsequent crack bridging events.
4. The comparison of J_b and J_{tip} contributions to the J_c clearly reveals that the J_b contributes 80–90% of the overall fracture energy and the actual contribution to the fracture energy from the crack tip fracture events are significantly small, if not negligible.
5. The fracture process in the crack divider direction was found to occur under stable conditions, validating all the three fracture toughness parameters evaluated in the present study. The same in the crack arrester direction is less deterministic as the fracture process after the fibre bundle failure occurs under apparent unstable conditions.
6. The J_R-curve effects, indicating the increase in fracture resistance with the extent of crack extension, are found to be more pronounced in the crack divider orientation as compared to the crack arrester orientations. The J_R-curve is significantly rising in nature in the crack divided orientation while the same in the crack arrester orientation is relatively flat.

Acknowledgements

The authors feel indebted to Dr. D. Banerjee, Director, DMRL for constant encouragement, active participation as well as numerous critical comments and valuable suggestions on this work. They thank him for the kind permission to publish the results. The authors would like to thank the DMRL scientists, Dr. J. Subramanyam and Dr. N. Ramakrishnan (presently the Director, RRL, Bhopal, India) for active participation in these studies. The authors gratefully acknowledge the financial support from Defence Research and Development Organisation (DRDO). The help received in material processing from Mr. Anil Kumar of ASL and Mr. N.V. Visweswara Rao of Ceramics and Composites Division, DMRL, is gratefully acknowledged.

References

[1] Clegg WJ, Kendall K, Alford NM, Button TW, Birchall JD. A simple way to make tough ceramics. Nature (London) 1990;347:455–7.
[2] Evans AG. Perspective on the development of high toughness ceramics. J Am Ceram Soc 1990;73:187–206.
[3] Campbell GH, Ruehle M, Dalgleish BJ, Evans AG. Whisker toughening: A comparison between aluminium oxide and silicon nitride toughened with silicon carbide. J Am Ceram Soc 1990;73:521–30.
[4] Becher PF. Microstructural design of toughened ceramics. J Am Ceram Soc 1991;74:255–69.
[5] Danial IM, Ishai O. Engineering mechanics of composite materials. London: Oxford University Press; 1994.
[6] Faber KT. Ceramic composite interfaces: Properties and design. Annual Rev Mater Sci 1997;27:499–524.
[7] Huseby IC, Borom MP, Greskovich CD. High temperature characterisation of silica-base cores for superalloys. Am Ceram Soc Bull 1979;58:448–52.
[8] Lewis G. Selection of engineering materials. Prentice Hall Inc.; 1990. p. 62–6.
[9] Ortiz-Lango CR, White KW. Elevated-temperature fracture characterization of advanced fibrous ceramic thermal insulators. J Am Ceram Soc 1994;77:2703–11.
[10] Visweswara Rao NV, Vijayakumar M. Silica fibre reinforced silica composites: Part I. Fabrication of composites, DMRL Technical Report DMRL TR 2000267 (Restricted). Defence Metallurgical Research Laboratory, Hyderabad, India, 2000.
[11] Shetty DK, Rosenfield AR, Duckworth WH. Fracture toughness of ceramics measured by a Chevron-notch diametral-compression test. J Am Ceram Soc 1985;68:C-325–7.
[12] Marshall DB, Oliver WC. Measurement of interfacial mechanical properties in fiber-reinforced ceramic composites. J Am Ceram Soc 1987;70:542–8.
[13] Zok F, Sbaizero O, Hom CL, Evans AG. Mode-I fracture resistance of a laminated fiber-reinforced ceramic. J Am Ceram Soc 1991;74:187–93.
[14] Clegg WJ. The fabrication and failure of laminar ceramic composites. Acta Metall Mater 1992;40:3085–93.
[15] Jessen TL, Bender BA, Lewis D. Mechanical properties of layered and laminated ceramic matrix composite systems. Ceram Engng Sci Proc 1993;13:796–803.
[16] Droillard C, Lamon J. Fracture toughness of 2-D woven SiC/SiC CVI-composites with multilayered interphases. J Am Ceram Soc 1996;79:849–58.
[17] Jessen TL, Greenhut VA, Lewis D, Friel JJ. Effect of microstructure on the mechanical behavior of continuous-fiber-reinforced ceramic–matrix composites. J Am Ceram Soc 1999;82:2753–61.
[18] Shaw LL. Measurement of the fracture energy of interfaces in composites through sandwich-type Chevron-notched specimens. J Testing and Eval 1997;25:391–9.
[19] Sakai M, Bradt RC. Fracture toughness testing of brittle materials. Inter Mater Rev 1993;38:53–78.
[20] ASTM Standard E-399. Standard test method for plane strain fracture toughness of metallic materials. Annual Book of ASTM Standards vol. 03.01. West Conshokochen, PA: American Society for Testing and Materials; 1997. p. 408–38.
[21] Rice JR. J Appl Mech, Trans ASME 1968;35:379–86.
[22] Begley JA, Landes JD. The J-integral as a fracture criterion; The effect of specimen geometry on J_{Ic}. In: Fracture toughness, ASTM STP No. 514; 1972. p. 1-23, 24–39.
[23] Landes JD, Begley JA. Test results from J-integral studies: An attempt to establish a J_{Ic} test procedure. In: Fracture analysis, ASTM STP No. 560; 1972. p. 170–86.
[24] ASTM Standard E-813. Standard test method for J_{Ic}, a measure of fracture toughness. Annual Book of ASTM Standards vol. 03.01. West Conshokochen, PA: American Society for Testing and Materials; 1997. p. 627–41.
[25] Sakai M, Ichikawa H. Work-of-fracture of brittle materials with microcracking and crack bridging. Int J Fract 1992;55:65–79.
[26] Li VC. Fracture resistance parameters for cementitious materials and their experimental determination. In: Shaw SP, editor. Application of fracture mechanics to continuous composites. Marinus Nijhoff Publications; 1985. p. 431–49.
[27] Li VC, Chan CM, Leung CKY. Experimental determination of the tension-softening curve in continuous composites. Ceram Concrete Res 1987;17:441–52.
[28] Li VC. Post-crack scaling relations for fiber reinforced cementitious composites. J Mater Civil Engng 1992;4:41–57.
[29] Hashida T, Li VC, Takahashi H. New development of the J-based fracture testing technique for ceramic–matrix composites. J Am Ceram Soc 1994;77:1553–61.
[30] Mai Y-W. Fracture and fatigue of non-transformable ceramics: The role of crack-interface bridging. In: van Mier JGM, Roes JG, Bakker A, editors. Fracture processes in concrete, rock and ceramics. London: E and FN Span; 1991. p. 3–26.
[31] Nair SV, Wang YL. Toughening behaviour of a two-dimensional SiC/SiC woven composite at ambient temperature: I, Damage initiation and R-curve behaviour; Wang YL, Nair SV. II, Stress–displacement relationship in the crack process zone. J Am Ceram Soc 1998;81:1149–56, pp. 1157–1162.
[32] Iyer KR, Milcot RB. Application of instrumented impact testing for studying dynamic fracture behavior of rotor steels. ASTM STP No. 563. Philadelphia, CA: American Society for Testing and Materials; 1974. p. 146–63.

[33] Broek D. Elementary engineering fracture mechanics. Nijhoff; 1985.
[34] Eswara Prasad N, Loidl D, Vijayakumar M, Kromp K. Elastic properties of silica–silica continuous fibre-reinforced, ceramic matrix composites. Scripta Mater 2004;50:1121–6.
[35] Newman JC. Notch sensitivity of space shuttle tile materials. Report No. NASA TM 81854. 1980.
[36] Green DJ, Lange FF. Micromechanical model for fibrous ceramic bodies. J Am Ceram Soc 1982;65:136–41.
[37] Green DJ, Ritter JE. Fracture behavior of low-density fibrous ceramics. J Am Ceram Soc 1982;65:141–6.
[38] Green DJ, Hawkins CA, Hirlinger MM. Double cantilever beam testing of a transversely isotropic fibrous silica material. J Am Ceram Soc 1983;66:46–9.
[39] Komine A, Kobayashi AS. Interfacial fracture of the space shuttle thermal protection system. Exp Mech 1982;22:454–61.
[40] Komine A, Kobayashi AS. Fracture behaviour of space shuttle thermal protection system. J Am Ceram Soc 1983;66:641–4.
[41] Nair SV, Wang YL. Failure behaviour of a 2-D woven SiC fiber/SiC matrix composite at ambient and elevated temperatures. Ceram Engng Sci Proc 1992;13:433–41.
[42] Jones RH, Steiner D, Heinisch HL, Newsome GA, Herch HM. Review: Radiation-resistant ceramic–matrix composites. J Nuclear Mater 1997;245:87–127.
[43] Xu YD, Cheng LF, Zhang LT. Strong and tough 3D textile C/SiC composites by chemical vapor infiltration. Mater Sci Engng 2001;A300:196–202.
[44] Xu YD, Cheng LF, Zhang LT, Yin HF, Yin XW. Microstructure and mechanical properties of three-dimensional textile Hi-Nicalon SiC/SiC composites by chemical vapor infiltration. J Am Ceram Soc 2002;85:1217–21.